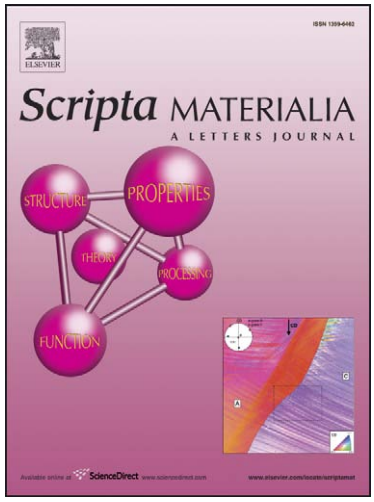

Large-scale synthesis of Al–Cu–Fe submicron quasicrystals

Laijun Li, Qinling Bi, Jun Yang, Licai Fu, Liping Wang, Shuncai Wang, Weimin Liu

PII: S1359-6462(08)00365-5
DOI: 10.1016/j.scriptamat.2008.05.008
Reference: SMM 7158

To appear in: *Scripta Materialia*

Received Date: 1 May 2008
Revised Date: 10 May 2008
Accepted Date: 11 May 2008

Please cite this article as: L. Li, Q. Bi, J. Yang, L. Fu, L. Wang, S. Wang, W. Liu, Large-scale synthesis of Al–Cu–Fe submicron quasicrystals, *Scripta Materialia* (2008), doi: 10.1016/j.scriptamat.2008.05.008

Large-scale synthesis of Al–Cu–Fe submicron quasicrystals

Laijun Li[a,c], Qinling Bi[a,*] ,Jun Yang[a,*] , Licai Fu[a,c], Liping Wang[a], Shuncai Wang[b], Weimin Liu[a]

[a] State Key Laboratory of Solid Lubrication, Lanzhou Institute of Chemical Physics, Chinese Academy of Sciences, Lanzhou 730000, China

[b] School of Engineering Sciences, University of Southampton, Southammpton SO17 1BJ, UK

[c] Graduate University of Chinese Academy of Sciences, Beijing 100039, China

*Corresponding author. Tel.:+86-931-4968193; fax: +86-931-8277088.

E-mail address: qlbi@lzb.ac.cn (Q. Bi), jyang@lzb.ac.cn (J. Yang).

Al–Cu–Fe alloy with a nominal composition of $Al_{62}Cu_{25.5}Fe_{12.5}$ (at.%) has been fabricated by a combination of pressure-assisted self-propagating high-temperature synthesis and rapid solidification. The as-synthesized Al–Cu–Fe alloy mainly consists of icosahedral quasicrystalline (IQC) ψ-$Al_{65}Cu_{20}Fe_{15}$ and cubic β-Al (Cu, Fe) solid solution phases, and exhibits finely equiaxed grains with a size ranging from 50 to 200 nm. The mechanism for the formation of the ultrafine-grained IQC phase has been explained.

***Keywords*:** Self-propagating high-temperature synthesis (SHS); Quasicrystals (QC); Al–Cu–Fe alloy; Ultrafine grained microstructure; Rapid solidification (RS).

Since the discovery of an icosahedral quasicrystalline (IQC) phase in rapidly solidified Al-Mn alloys [1], quasicrystalline (QC) materials have attracted considerable attention owing to their excellent physical, chemical, mechanical and tribological properties, such as high hardness, enhanced elastic modulus, very low friction coefficient,

low surface energy, supercorrosion and wear resistance, and low electrical and thermal conductivity. Due to their thermodynamic stability, non-toxicity and low production cost, Al–Cu–Fe QC materials have great potential for practical applications in areas such as thermal barrier coatings, low-friction wear-resistant coatings, composite biomaterials and catalysts, and as reinforcement phases/fillers for composite materials [2-4].

In previous studies, Al–Cu–Fe QC materials were synthesized via magnetron sputtering, physical vapor deposition, melt spinning, mechanical alloying as well as atomization techniques [4-9]. The samples prepared by the above techniques were in the forms of ribbons, thin films or powders, and were annealed in vacuum to improve the volume fraction of IQC phase. However, for potential large-scale applications of these quasiperiodic materials, high-efficiency and low-cost synthesis techniques are needed.

Pressure has been used to produce nanocrystalline materials, because it can decrease the potential barrier for nucleation and increase the diffusion activation energy [10]. In addition, pressure or electric field-activated sintering facilitates the synthesis of single-phase Al–Cu–Fe IQC materials [11, 12]. The objective of the present work is to develop a new one-step production approach for the large-scale synthesis of Al–Cu–Fe IQC materials through a combination of pressure-assisted self-propagating high-temperature synthesis (SHS) and rapid solidification (RS). This method offers a particular advantage in the preparation of the IQC materials, as the rapid quenching under pressure facilitates the precipitation of nano-sized IQC phase from the deeply supercooled melt (SCM). To fabricate the Al–Cu–Fe IQC material, an aluminothermic reaction (1) has been designed to prepare superheated melt. Iron and aluminum powders are added to reduce the adiabatic combustion temperature and thus avoid vaporization of constituents. Since the Al–Cu–Fe melt is in a highly superheated liquid state after the

completion of combustion reaction, the number of heterogeneous nucleation sites is reduced. Accordingly, the RS of the deeply SCM under pressure gives rise to the formation of an ultrafine-grained microstructure.

$$3CuO + 2Al = Al_2O_3 + 3Cu + 1194.4kJ / mol \qquad (1)$$

Aluminum, copper oxide and iron powders were weighed according to the stoichiometry of Eq. (2) to produce Al–Cu–Fe QC material with a nominal composition of $Al_{62}Cu_{25.5}Fe_{12.5}$. The characteristics of the reactant powders are given in Table 1.

$$79Al + 25.5CuO + 12.5Fe = 8.5Al_2O_3 + Al_{62}Cu_{25.5}Fe_{12.5} \qquad (2)$$

The powders were dry-mixed for 4 h in a planetary ball mill using a stainless steel vial and alumina balls at 180 rpm. The ball-to-powder mass ratio was 1:5. The mixed powders were then cold-pressed in a copper mold. A powder mixture consisting of Al, S and MnO_2 was pressed into a pellet as an igniter. The igniter was put on top of the pressed reactant powders. The copper mold with the reactants was placed in a SHS reactor. The reactor was purged with argon gas at room temperature, and was then heated after the introduction of 8 MPa argon gas. The reaction of the igniter was started as the reactor reached about 260 °C. The released heat induced the reaction shown in Eq. (2) and the synthesis reaction was subsequently finished in a few seconds. The resulting Al–Cu–Fe sample was about 6 mm in thickness and 60 mm in diameter. The black alumina was on the top of the target product, and separated naturally from the desired Al–Cu–Fe sample.

Phase identification was carried out by X-ray diffraction (XRD), using a Philips, X'Pert-MRD diffractometer with Cu K_α radiation. Differential thermal analysis (DTA) was conducted under a flowing purified argon atmosphere using a Diamond calorimeter

(Perkin Elmer) at a heating rate of 20 °C min^{-1} to determine the temperature of the phase transformation. The XRD measurement and thermal analysis of the as-fabricated Al–Cu–Fe alloy were performed using powder samples prepared from the brittle bulk by crushing in a mortar. The microstructural features of the as-fabricated Al–Cu–Fe samples were examined by transmission electron microscopy (TEM) using a Hitachi 600 microscope operating at 100 kV. The foils for TEM observations were prepared by dispersing crushed sample fragments on microgrids covered with a porous carbon film [13].

Figure 1 presents a continuous DTA trace for the as-fabricated Al–Cu–Fe powder at a heating rate of 20 °C min^{-1} after calibration. Three endothermic peaks are observed at temperatures of 648, 882 and 979 °C, which are consistent to the melting temperatures of the φ-$Al_{10}Cu_{10}Fe_1$, ψ-IQC-$Al_{65}Cu_{20}Fe_{15}$ and cubic β-Al (Cu, Fe) solid solution phase, respectively [14]. The crystallographic data of these phases are listed in Table 2 [15, 16]. The enthalpy of the first minimum peak is smaller than those of the other two peaks, which indicates that the concentration of the φ phase is much lower.

Figure 2 shows the XRD pattern of the as-fabricated Al–Cu–Fe alloy. The peaks corresponding to the IQC and β phases were indexed using Cahn (N, M) indices [17] and Miller indices, respectively. Some much smaller peaks are also observed and they may be from the φ phase evidenced by the thermal analysis. The φ phase was not indexed as its JCPDS card is not available. Using an peak-fitting program (Jade 5.0), the volume fractions of the IQC and crystalline phases have been calculated by the ratio of sum of integrated areas of all Bragg diffraction peaks for the corresponding phases [18,19]. The resultant volume fractions of the IQC, β and φ phases were calculated to be about 68, 30

and 2%, respectively. The six-dimensional (6-D) quasilattice parameter of the IQC phase was calculated by a Cohen–Wangner extrapolation procedure[20]:

$$a_{6d} = d\sqrt{\frac{N + M\tau}{2(2+\tau)}} \qquad (3)$$

where (N, M) are the Cahn indices of diffraction peaks, d is the interplanar spacing, and τ is the golden ratio (τ = 1.618). The calculated 6-D lattice parameter was about 0.6321 nm, which is in good agreement with the value of the lattice parameter for the Al–Cu–Fe face-centered icosahedral coating [6].

Figure 3 shows typical TEM images and corresponding selected-area electron diffraction (SAED) pattern taken from the thin region of the foils of the Al–Cu–Fe alloy. Finely equiaxed grains with a size ranging from 50 to 200 nm can be observed (Fig. 3a and b). The grain size of the as-fabricated sample is smaller than that of the $Al_{65}Cu_{20}Fe_{15}$ coating prepared by electron beam physical vapor deposition (200-400 nm) [21]. From the SAED pattern, the ratios of the radii of the third to the first ring and of the forth to the second ring were found to be equivalent to the golden mean (1.618); this confirmed that these rings belong to the IQC phase [19] (the a, b, c, d, e rings correspond to the (16, 24), (20, 32), (40, 64), (52 ,84), (80, 128) planes of the IQC phase).

The adiabatic combustion temperature of the aluminothermic reaction was calculated to be about 4878 °C [22]. After the addition of aluminum and iron powders, it decreases to about 2930 °C. The Al–Cu–Fe alloy and alumina are in a highly superheated liquid state at this temperature. The liquid alumina might be immiscible with the Al–Cu–Fe melt and so be present in the form of molten drops which might become dispersed in the melt. The drops apparently tend to coalesce into bigger drops by collision, thereby lowering the interfacial energy. The high volume fraction of the drops contributes

to the high probability of collision, and the low viscosity of the melt facilitates the diffusion of the drops [23]. Both factors enhance the coalescence velocity, and the drops may coalesce into even bigger drops which could be left on top of the melt. As a consequence, the alumina is separated from the melt, and the molten Al–Cu–Fe alloy is deposited on the substrate surface.

Icosahedral short-range order is common in SCMs and has a profound effect on the phase selection during the solidification of SCMs. The structural similarity between the melt and the IQC phase gives a dramatically lower solid–liquid interfacial energy. The dimensionless solid–liquid interfacial energies of IQC, β and φ phases are 0.3, 0.63 and 0.86, respectively [24, 25]. Obviously, the interfacial energy of IQC phase is the lowest. According to the classical nucleation theory, the lower the interfacial energy, the lower nucleation work is; in other words, the nucleation of the IQC phase is preferable. Therefore, the IQC phase precipitates primarily from the rapidly quenched Al–Cu–Fe melt. Due to the release of latent heat of solidification, the cooling rate gradually decreases; while it is smaller than the critical cooling rate, the β phase forms from the SCM accompanied by the IQC phase. It has been reported that the IQC phase crystallizes by a precipitation mechanism at higher cooling rates [26]. Molecular dynamics simulation has also corroborated that the IQC phase spontaneously nucleates from the deeply SCM, and a QC nucleus grows by assimilating icosahedral clusters whose formation is favored in a supercooled liquid [27, 28]. The φ phase may be formed by a solid-state decomposition reaction that converts the supersaturated β solid solution phase into the ordered B2 and the φ phases [14]. Because the precipitation of the φ phase is controlled by diffusion, in which the diffusion of atoms becomes sluggish in the solid

state, the content of the φ phase is much lower.

The majority of low-boiling-point contaminants introduced from the igniter and reactants may be vaporized owing to the high adiabatic combustion temperature. The by-product, alumina, which was used to act as nucleation sites for the IQC and β phases, might be lifted to the top of the melt by the superheating treatment. The numbers of heterogeneous nucleation sites could be reduced; as a result, the temperature of the onset crystallization may shift to even lower temperatures and the thermodynamic undercooling could be greatly increased. In addition, kinetic undercooling increases due to the rapid quenching rate [29]. Since the nucleation rate increases dramatically with increased undercooling, and the radii of critical nuclei are inversely proportional to the undercooling, the enhanced nucleation rate and decreased radii of critical nuclei refine the solidified microstructure. Furthermore, the growth rate of the IQC phase is far smaller than that of the crystalline phase [25], and the time of nuclei growth is shorter because of the high cooling rate resulting from the copper substrate quenching [30-32]. These factors also contribute to the formation of refined IQC grains.

The applied pressure plays a crucial role in the nucleation and growth of the IQC phase. As the potential barrier for nucleation decreases with an increase in chamber pressure [10, 33], when the deeply SCM crystallizes under pressure, the thermodynamic potential barriers for the IQC and β phases nucleation could be lowered, and the nucleation rates could be enhanced. On the other hand, the pressure can suppress the growth of the nuclei in the SCM, since applied pressure can increase the diffusion activation energy of the SCM, and long-range atomic diffusion in the SCM can be inhibited by the lower atomic mobility [10]. This makes the growth of the nuclei of the

IQC and β phases more difficult. A number of studies have confirmed that applied pressure during the solidification process, of the order of either GPa or Pa, suppresses the diffusivity of atoms in deeply SCMs [10, 34, 35], hence resulting in the formation of ultrafine-grained microstructures. Moreover, rapid quenching under pressure can also facilitate the formation of the IQC phase, because the external pressure may influence the sequence of solid-state interdiffusion reactions. For example, a single-phase bulk Al–Cu–Fe QC material has been prepared by a field-activated sintering technique under an applied pressure of 55 MPa [36]. In summary, the formation of ultrafine grains might be attributed to the copious nucleation and slow growth rate induced by pressure-assisted rapid quenching.

The $Al_{62}Cu_{25.5}Fe_{12.5}$ alloy with grain sizes in the range of 50-200 nm has been obtained using a combination of pressure-assisted SHS and RS. The as-fabricated Al–Cu–Fe alloy mainly consists of the IQC and β phases. By rapid quenching under pressure, the deeply SCM undergoes a non-equilibrium solidification process which leads to the formation of an ultrafine-grained microstructure. In addition, the pressure-assisted rapid quenching enhances the QC-forming ability of the Al–Cu–Fe alloy, and thus the content of the IQC phase is enhanced. The present result also demonstrates that the combination of pressure-assisted SHS and RS is a promising industrial synthesis approach for fabricating Al–Cu–Fe IQC materials.

The authors are grateful to the National Natural Science Foundation of China (50432020), the National 973 project of China (2007CB607601), the Innovation Group Foundation from NSFC (50421502) for financial support.

[1] D. Shechtman, I. Blech, D. Gratias, J.W. Chan, Phys. Rev. Lett. 53 (1984) 1951.

[2] J.M. Dubois, Mater. Sci. Eng. A 294-296 (2000) 4.

[3] E. Huttunen-Saarivirta, J. Alloy. Compd. 363 (2004)150.

[4] A. Inoue, Prog. Mater. Sci. 43 (1998) 365.

[5] E.J. Widjaja, L.D. Marks, Thin Solid Films 420-421 (2002) 295.

[6] A.I. Ustinov, B.A. Movchan, S.S. Polishchuk, Scripta Mater. 50 (2004) 533.

[7] G. Rosas, R. Perez, Mater. Lett. 47 (2001) 225.

[8] V.V. Tcherdyntsev, S.D. Kaloshkin, E.V. Shelekhov, A.I. Salimon, S. Sartori, G. Principi, Intermetallics 13 (2005) 841.

[9] A.V. Krajnikova, V.V. Likutina, G.E. Thompsonb, Appl. Surf. Sci. 210 (2003) 318.

[10] Y.X. Zhuang, J.Z. Jiang, T.J. Zhou, H. Rasmussen, L. Gerward, M. Mezouar, W. Crichton, A. Inoue, Appl. Phys. Lett. 77 (2000) 4133.

[11] F. Turquier, V.D. Cojocaru, M. Stir, R. Nicula, C. Lathe, E. Burkel, Rev. Adv. Mater. Sci. 8 (2004)147.

[12] R. Nicula, M. Stir, F. Turquier, E. Burkel, Mater. Sci. Eng. A 475 (2008) 113.

[13] W. Sun, T. Ohsuna, K. Hiraga, J. Alloy. Compd. 342 (2002) 87.

[14] L.M. Zhang, J. Cshneider, R. Lück, Intermetallics 13 (2005) 1195.

[15] F. Hippert, R.A. Brand, J. Pelloth, Y. Calvayrac, J. Phys.:Condens. Matter. 6 (1994) 1189.

[16] E. Belin-Ferré, V. Fournée, J.M. Dubois, J. Phys.:Condens. Matter. 12 (2000) 8159.

[17] J.W. Cahn, D. Schechtman, D. Gratias, J. Mater. Res. 1 (1986) 13.

[18] L.C. Zhang, Z.Q. Shen, J. Xu, J. Mater. Res. 18 (2003) 2141.

[19] P. Barua, B.S. Murty, B.K. Mathur, V. Srinivas, J. Mater. Res. 17 (2002) 653.

[20] J.L. Joulaud, M.J. Captián, D. Haüserman, S. Lefebvre, Y. Calvayrac, Phys. Rev. B 59 (1999) 3521.

[21] Y.V. Milman, D.V. Lotsko, S.N. Dub, A.I. Ustinov, S.S. Polishchuk, Ulshin, Surf. Coat. Tech. 201 (2007) 5967.

[22] G.B. Schaffer, P.G. McCormick, Metall. Trans. A 21 (1990) 2789.

[23] M. V. Smoluchowsky, Z. Phys. Chem. 92 (1917) 129.

[24] D. Holland-Moritz, T. Schenk, V. Simonet, R. Bellissent, Philo. Mag. 86 (2006) 255.

[25] D. Holland-Moritz, J. Schroers, D.M. Herlach, B. Grushko, K. Urban, Acta Mater. 46 (1998) 1601.

[26] D. Holland-Moritz, J. Schroers, B. Grushko, D.M. Herlach, K. Urban, Mater. Sci. Eng. A 226-228 (1997) 976.

[27] P.J. Steinhart, Nature 452 (2008) 43.

[28] A.S. Keys, S.C. Glotzer, Phys. Rev. Lett. 99 (2007) 235503.

[29] J. Mahmoudi, H. Fredriksson, Mater. Sci. Eng. A 226-228 (1997) 22.

[30] P.Q. La, J. Yang, J.H. David, W.M. Liu, Q.J. Xue, Y.D. Li, Adv. Mater. 18 (2006) 733.

[31] J. Yang, J.Q. Ma, W.M. Liu, Q.L. Bi, Q.J. Xue, Scripta Mater. 58 (2008) 1074.

[32] L.J. Li, Q.L. Bi, J. Yang, W.M. Liu, Q.J. Xue, Mater. Lett. 62 (2008) 2458.

[33] X.J. Gu, F. Ye, F. Zhou, K. Lu, Mater. Sci. Eng. A 278 (2000) 61.

[34] W.H. Wang, C. Dong, C.H. Shek, Mater. Sci. Eng. R 44 (2004)45.

[35] A.D. Setyawan, H. Kato, J. Saida, A. Inoue, Mater. Sci. Eng. A 449-451 (2007) 903.

[36] R. Nicula, F. Turquier, M. Stir, V.Y. Kodash, J.R. Groza, E. Burkel, J. Alloy. Compd.

232 434-435 (2005) 319.

The list of figure and table captions

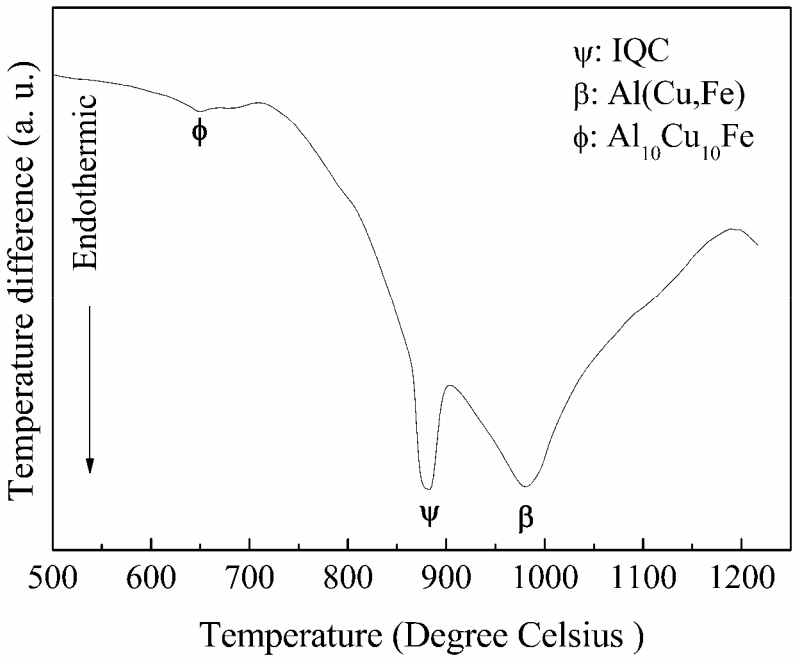

240

241 Fig. 1 A continuous DTA trace of the as-fabricated Al–Cu–Fe alloy.

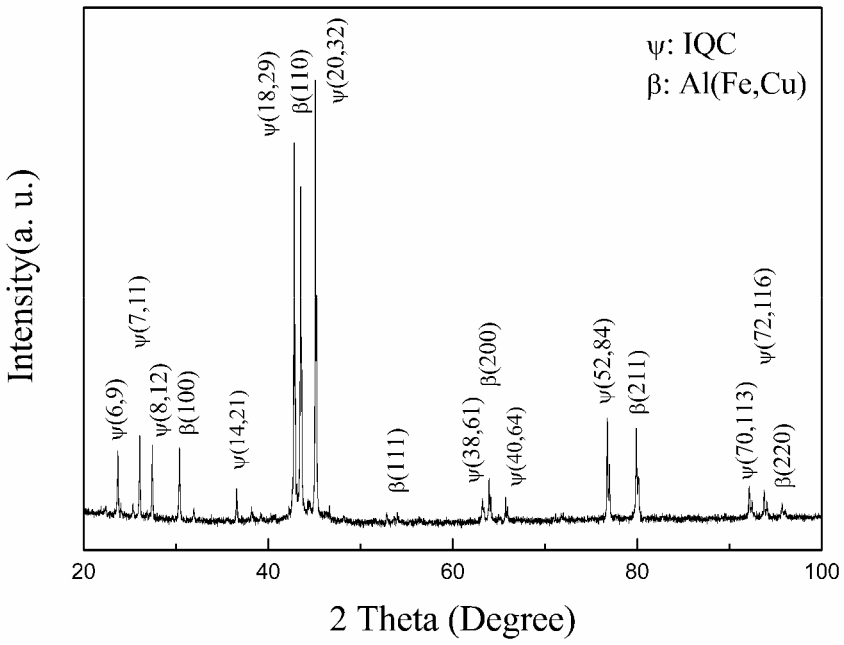

242

243 Fig. 2 The typical XRD pattern of the as-fabricated Al–Cu–Fe alloys.

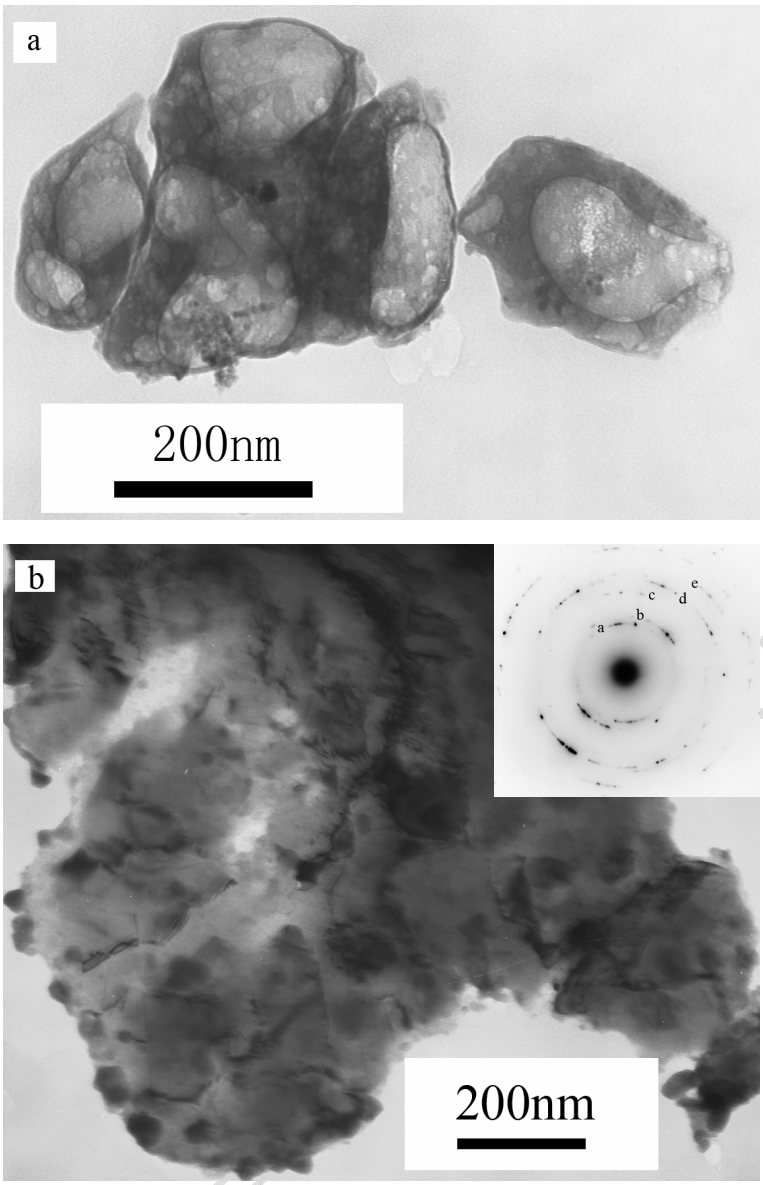

Fig. 3 The typical TEM images (a, b) of the Al–Cu–Fe alloy. The inset is the corresponding selected area electron diffraction pattern.

256 Table 1. Chemical and physical properties of the raw material powders.

Powder	Size (mesh)	Purity (wt%)	Impurity
Al	100-200	>99.0	Fe, Si, Cu, H_2O
CuO	100-200	>99.0	Fe, Cu_2O
Fe	200	>98.0	Cu, N, S, H_2O

257

Table 2 Crystallographic characteristics of the IQC, φ and β phases.

Phase	***Lattice***	***Lattice parameters(Å)***
IQC-$Al_{65}Cu_{20}Fe_{15}$	Icosahedral	a_{6D} = 6.3176
φ-$Al_{10}Cu_{10}Fe$	Hexagonal	a = 4.106, c = 5.095
β-Al(Cu, Fe)	B2(CsCl)	a = 2.910